Jpn. J. Appl. Phys. Vol. 35 (1996) pp. 4503–4508
Part 1, No. 8, August 1996

# Effects of Axial Magnetic Field and Faraday Shield on Characteristics of RF Produced Plasma Using Spiral Antenna

Shunjiro SHINOHARA* , Seiji TAKECHI and Yoshinobu KAWAI
*Interdisciplinary Graduate School of Engineering Sciences, Kyushu University, Kasuga, Fukuoka 816, Japan*

(Received December 8, 1995; accepted for publication May 2, 1996)

Influences of the axial magnetic field and Faraday shield on the performance of RF produced plasma using a spiral antenna are investigated. The RF power and filling pressure dependences, antenna-plasma coupling, Ar line intensities and spatial profiles of plasma parameters are studied. With the magnetic field and/or without a Faraday shield, the threshold input power for plasma initiation is lowered and the antenna-plasma coupling is improved. In addition, a collisionless heating mechanism is suggested. With the increase in the applied magnetic field, the ion saturation current increases and shows a peaked radial profile; in the low-pressure range it shows a nearly flat axial profile.

KEYWORDS: RF plasma, ICP, spiral antenna, magnetic field, Faraday shield, impurity, helicon wave

## 1. Introduction

For material processing and toroidal confinement devices, a convenient high-density plasma source at low pressure has been urgently required. A helicon wave plasma[1–7] and inductively coupled plasma/transformer coupled plasma (ICP/TCP)[8] have been demonstrated to fulfill for example, dry etching requirements, in the RF range, and some basic studies on plasma and wave characteristics have been conducted. Recently, a planar, spiral coil[9–11] has been used in ICP due to the advantage of relatively simple geometry, but limited empirical characterization has been carried out and there remain some problems to be solved regarding the antenna-plasma coupling, plasma characteristics and RF wave phenomenon.

In some cases, capacitive (electrostatic) coupling is observed with low RF power, in contrast with the inductive coupling obtained with high RF power,[12] which is associated with the density jump. For checking these different discharge regions, antenna-plasma coupling studies are important. The role of the Faraday shield,[11,13] which is expected to reduce capacitive coupling if it exists, by lowering the radial ($r$) and axial ($z$) electric fields in the cylindrical geometry, must also be investigated in order to alleviate the phenomenon of sputtering from the antenna window. In addition, data of the coupling coefficient (power transmission efficiency: the ratio of the net power absorbed by the plasma to the input RF power), which is very important from the viewpoint of required minimum RF power and lowering of antenna voltage, have rarely been reported up to now. In this study, experimentally obtained resistance (coupling) is compared with those obtained from collisional and collisionless electron heating models[14] with changing collision frequency.

If we add a static axial magnetic field, which has not yet been done as far as we know, radial diffusion can be altered and a propagating wave, in contrast to the evanescent wave in the ICP case, may be excited in certain cases. These two factors, namely, diffusion and a propagating wave, contribute to a change of plasma parameters, which means that this magnetic field can be an additional control parameter for the plasma discharge. Here in this work, we will focus on the effects of the axial magnetic field and Faraday shield (and also input RF power and filling pressure) on the plasma characteristics, including the antenna-plasma coupling and wave phenomena, with the use of a spiral antenna.

*E-mail: shinoigh@mbox.nc.kyushu-u.ac.jp

## 2. Experimental Setup

The experimental system is shown in Fig. 1. Near the antenna, Ar gas is fed into the left side of the vacuum chamber, and the static axial magnetic field of $B < 200$ G is applied if necessary. Here, $z = 0$ cm is defined at the right-side surface of a quartz window 25 cm in diameter with 0.8 cm thickness. The four-turn, water-cooled, spiral antenna with 18 cm diameter is made of copper,

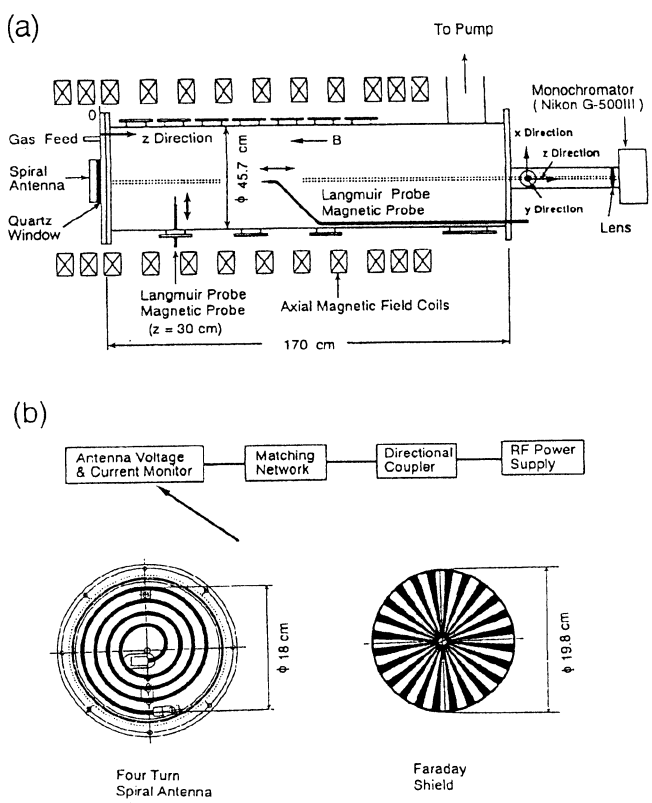


Fig. 1. Schematic views of (a) the experimental apparatus and (b) the antenna structure including the RF system.

and the copper Faraday shield (FS) 0.2 cm thick can be put on this antenna to be expected to reduce the radial and axial components of the electric field. The spacing between FS and the window is 0.6 cm and the distance between the surfaces of the antenna and window is 1.7 cm both with and without FS.

The RF power and frequency are $< 5$ kW and 7 MHz, respectively, and RF output is continuous (in some cases, pulse width is 5 ms with a duty of $\leq 0.25$ for protection from thermal damage). The RF power supply is connected to the antenna through a directional coupler, which picks up the incident and reflected power, i.e., $P_{inc}$ and $P_{ref}$, a matching box (split tank circuit) and monitors for antenna voltage and current between the antenna and matching box. Plasma parameters are measured by movable Langmuir and magnetic probes inserted into the plasma radially and axially. In addition, a visible monochromator (focal length is 50 cm) is located at the right side of the vacuum chamber to detect the light from the central part of the plasma; the maximum length in the $x$ direction observed using this monochromator, with a convex lens (focal length is 5.7 cm, the distance from the slit of the monochromator is 6 cm) and a metallic cylinder (inner tube radius is 7 cm), is $\sim 0.8$ cm throughout the vacuum chamber, which is illustrated in Fig. 1(a).

## 3. Parameter Dependence

Figure 2 shows coupling coefficient $\eta = R_p/(R_p + R_v)$, ion saturation current $I_{is}$, and Ar I (419.8 nm) and Ar II (488.0 nm) line intensities as a function of input RF power $P_{inp}$ $(= P_{inc} - P_{ref})$. Here, $R_v$ $(\sim 0.025\,\Omega)$ and $R_p$ are vacuum and plasma loading resistances, respectively, and effective inductance $L$ of the antenna is $\sim 0.47\,\mu$H. From signals of the directional coupler and antenna voltage and current, loading resistances, $R_v$ and $R_p$, and $L$ are derived, and $R_v(L)$ with FS is found to be larger (smaller) than that without FS by several %. Hence the net power $P_{net}$ absorbed by the plasma can be written as $\eta P_{inp}$. According to the results for four cases, i.e., with and without magnetic fields of $B = 36$ G as well as with and without Faraday shields, there exist the following features. 1) High coupling efficiency $\eta$ of $> 0.6$ which is nearly independent of $P_{inp}$ except in the low input power region ($< 0.5$ kW). This $\eta$ is higher without FS and/or with the magnetic field $B$. 2) In the presence of $B$, $I_{is}$ is larger by a factor of $\sim 3$ compared with that without $B$. For the case of without FS and with $B$ for $P_{inp} > 2$ kW, $I_{is}$ tends to saturate. 3) Ar I intensities are nearly the same for all cases, except for that with FS and $B$ of $P_{inp} > 2$ kW. 4) The rate of Increase in Ar II intensity with $P_{inp}$ is higher than those of $I_{is}$ and Ar I intensity, and Ar II intensities are also nearly the same in all cases, except for that with FS and $B$ where $P_{inp} > 0.5$ kW, in which it is larger than in other cases by a factor $< 10$. 5) The threshold power $P_{th}$ to initiate the plasma is nearly zero with $B = 36$ G, but without $B$, $P_{th}$ is $\sim 0.2$ kW and $\sim 0.85$ kW without and with FS, respectively.

As can also be seen in Fig. 2, we do not observe the density jump[12] but continuous density increase with the increase in the input power is seen ($P_{th}$ is very low, on the order of 10 W, with $B$, which is useful for controlling the plasma density from very low to high values continuously). Note that $I_{is}$ obtained experimentally is considered to be nearly proportional to electron density $n_e$ where electron temperature $T_e$ changes slightly. The antenna inductance $L$ is weakly dependent on the input power $P_{inp}$, filling pressure $P$ and the magnetic field $B$, and normalized inductance change $\Delta L/L$ is small of $-0.05$–$0.15$. There is a tendency for this inductance change to be higher (positive side) for cases without FS and/or with $B$. These results show that capacitive coupling is small, even for the low-power case in our experiments. However, in the absence of $B$, the lower $P_{th}$ value without FS compared to that with FS, may be due to some penetration of capacitive fields and/or the presence of three components of excited electric fields instead of only the main azimuthal component to help initiate the discharge.

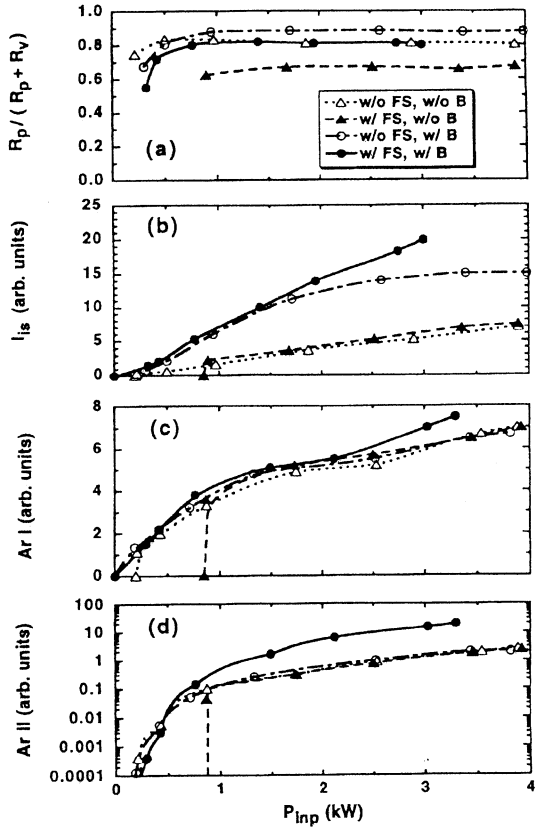


Fig. 2. Dependences of (a) coupling efficient $\eta = R_p/(R_v + R_p)$, (b) ion saturation current $I_{is}$ at $z = 30$ cm and $r = 0$ cm, (c) Ar I and (d) Ar II line intensities on the input RF power $P_{inp}$ under four different conditions. Here, filling pressure $P$ is 27 mTorr and the magnetic field $B$ is 36 G.

In order to check impurity release from the window or the vacuum vessel, we attemp to detect lines such as those of Si, O, N and Fe using a monochromator, but they are not found at a detectable level, even in the absence of FS. This is consistent with the abovementioned results of inductive coupling under all of the present experimental conditions, and contamination and etching of the window is not observed after these series of experiments. The reason why we succeed in high-density plasma production (up to $> 10^{13}\,\mathrm{cm}^{-3}$) with

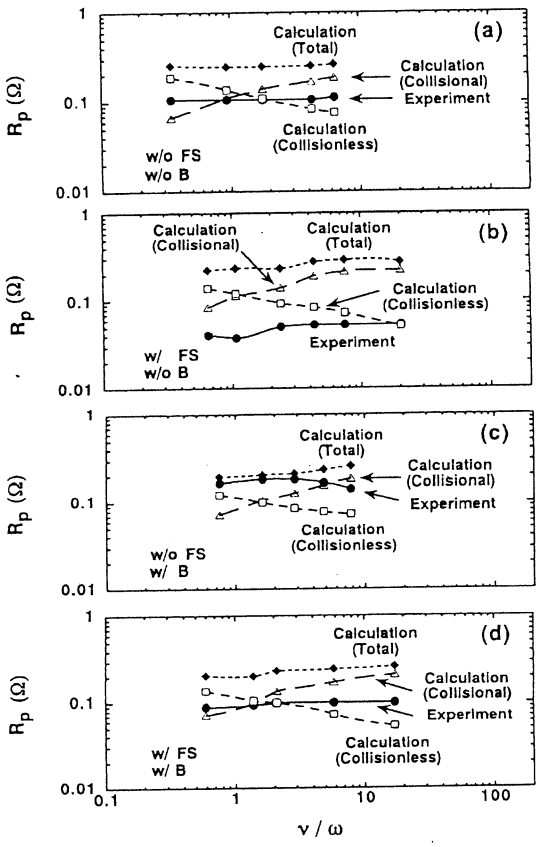


Fig. 3. Plasma loading resistance $R_p$ as a function of $\nu/\omega$ ($\nu$: sum of electron-neutral elastic and electron-ion coulomb collision frequencies, $\omega$: applied RF angular frequency of $2\pi \times 7$ MHz) under the four different conditions ($P_{inp} \leq 2$ kW). For comparison, values of $R_p$ estimated from collisional and collisionless (anomalous) heating models are shown in addition to the sum (total) of $R_p$ from the two models.

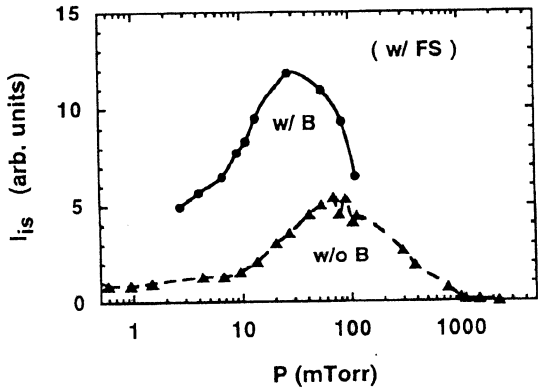


Fig. 4. Relationship between ion saturation current $I_{is}$ at $z = 30$ cm and $r = 0$ cm and filling pressure $P$ with and without the axial magnetic fields of $B = 36$ G, in the presence of the Faraday shield ($P_{inp} \sim 2$ kW).

no deleterious effects even without FS is not clear, but the distance between the antenna and window surfaces (1.7 cm) and the average power density ($\sim 1.3\,W/cm^2$ for $P_{net} = 1.6$ kW) may be important.

Next, the dependence of the plasma loading resistance $R_p$ on normalized collision frequency $\nu/\omega$ is studied under four sets of conditions, changing the filling pressure $P$, as shown in Fig. 3 ($\nu$: sum of electron-neutral elastic[15] and electron-ion[16] coulomb collision frequencies; $\omega$: applied RF angular frequency of $2\pi \times 7$ MHz). Here, $\nu$ is derived from $T_e$ (measured at $z = 30$ cm) and $n_e$, which is estimated from the data of $I_{is}$ near the plasma surface at $z = 3$ cm and of $T_e$ at $z = 30$ cm ($T_e$ is slightly higher near the antenna side than that away from the antenna under our experimental conditions). When we consider the error in $T_e$, $\nu/\omega$ and estimated values of $R_p$ per unit antenna area (from collisional and collisionless (anomalous) heating models[14]) may change by less than 20%, which does not affect the conclusion below. For the collisional model, the real part of surface impedance is rewritten as $\mu_0\omega(c/\omega_p)\{(1-\phi)/2\phi\}^{0.5}$ from eq. (4) in ref. 14 under the condition that system size $L$ is such that $kL \gg 1$ ($k$ is defined in eq. (5)), and we use eq. (9) in the same reference for the collisionless model ($\mu_0$: permeability in the vacuum, $\omega_p$: plasma angular frequency, $c$: velocity of light, $\phi = \{1 + (\nu/\omega)^2\}^{-0.5}$).

Figure 3 shows that experimental antenna loading $R_p$ is weakly dependent on $\nu/\omega$, and this $R_p$ is higher without FS and/or with the magnetic field $B$, as mentioned above. In the experimental $\nu/\omega$ region, the behavior of total $R_p$ from two models (sum of the loading resistances) is similar to the experimental one for all cases. In the high $\nu/\omega$ region, the collisional model is expected to play an important role. However, in the low $\nu/\omega$ region, this model, which yields a low $R_p$ value, cannot explain the experimental loading, but the collisionless model seems to be consistent with the experimental result. This suggests that the collisionless electron heating[14] model is a candidate for explaining the RF heating mechanism in the low collisionality region. The ratio of anomalous skin depth to the collisional one (0.4–0.8 cm) is less than 1.4 in this experiment.

Figure 4 shows the relationship between the ion saturation current $I_{is}$ and filling pressure $P$ with and without the magnetic fields, in the presence of FS at $z = 30$ cm ($P_{inp} \sim 2$ kW). For simplicity, the two cases without FS (with and without the magnetic fields) are not shown, since there are no appreciable differences between the cases with and without FS. $I_{is}$ is about three times larger when the magnetic field ($B = 36$ G) is present, but initiation of the plasma tends to be difficult in the low ($< 2$ mTorr) and high ($> 100$ mTorr) pressure regions in the presence of $B$, especially with FS. The dependence of $n_e$ on $P$ is similar to that shown in Fig. 4 (the maximum density is $\sim 5 \times 10^{12}\,cm^{-3}$ with the magnetic field $B = 36$ G at $z = 30$ cm), and a slight decrease in $T_e$, ranging from about 2 to 3 eV, with $P$ is found in all four cases (with and without FS and $B$). The space potential $V_{sp}$ decreases slightly with the filling pressure (8–15 V in the four cases).

In order to see the effect of the magnetic field, $I_{is}$, Ar I and Ar II line intensities are measured as a function of $B$, as shown in Fig. 5. With an increase in $B$, $I_{is}$ increases almost linearly both with and without FS, and there is a tendency for $I_{is}$ to saturate when $B$ is above $\sim 100$ G in both cases. Although a slowly decreasing trend with nearly the same values is found for Ar I intensity in both cases, there is a difference in Ar II intensities between the two cases. This may be attributed to the differences

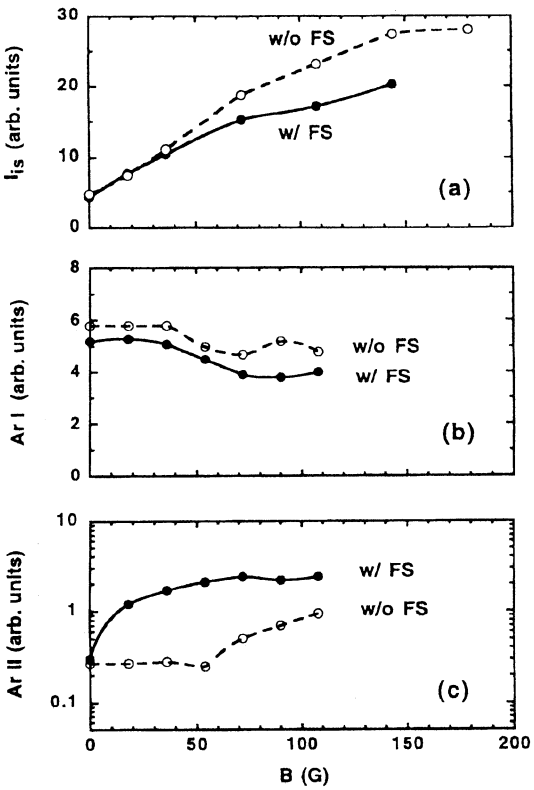


Fig. 5. Dependences of (a) ion saturation current $I_{is}$ at $z = 30$ cm and $r = 0$ cm, (b) Ar I and (c) Ar II line intensities on the axial magnetic field $B$ with and without the Faraday shield ($P = 27$ mTorr and $P_{inp} \leq 2$ kW).

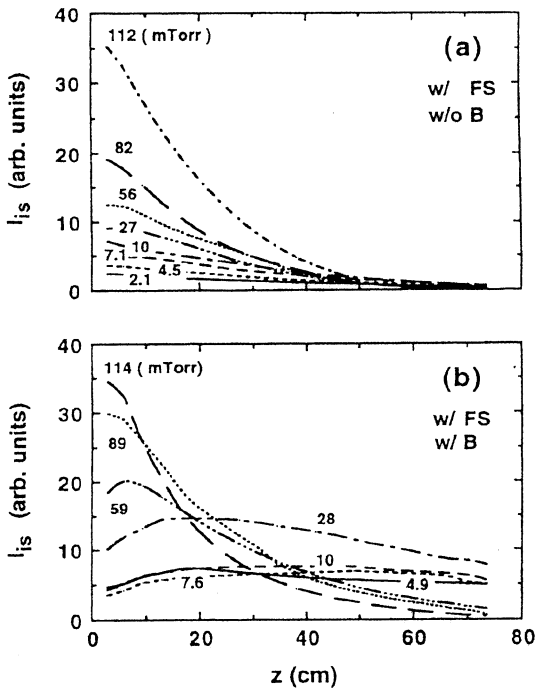


Fig. 6. Axial profiles of ion saturation current $I_{is}$ ($r = 0$ cm, $P_{inp} \sim 2$ kW) for cases (a) without and (b) with the axial magnetic fields $B$ of 36 G, in the presence of the Faraday shield, with various filling pressures $P$.

in $n_e$, $n_0$ (neutral density) and $T_e$ profiles (in the axial direction) near the plasma center, which contribute to the emission intensity profile, based on the fact that, *e.g.*, the plasma decays along the $z$ axis without FS for $B < 50$ G and is distributed nearly uniformly with FS and B in a low-pressure region.

For the case without FS shown in Fig. 5, Ar II intensity changes slightly for $B < 50$ G and increases when $B > 50$ G, which corresponds to the region of increasing amplitude of a helicon wave (wave character will be discussed in the next section). The increase in $I_{is}$ with $B$ is considered to be due to the combined effects of the improved plasma confinement and the presence of a propagating wave. Here, global experimental energy confinement time, which is defined as the ratio of total plasma energy to net RF power, without the magnetic field is estimated to be $\leq 10\,\mu$s for $P \sim 40$ mTorr.

## 4. Spatial Profile

Figure 6 shows a comparison of axial $I_{is}$ profiles for cases with and without the magnetic fields ($B = 36$ G) in the presence of FS. The same trend as shown in Fig. 6(a) is also obtained for cases without FS and without $B$, and without FS and with $B$ ($= 36$ G). Here, $n_e$ at $z \sim 15$ cm and $P = 28$ mTorr in Fig. 6(b) is as high as $8 \times 10^{12}$ cm$^{-3}$ ($T_e \sim 2$ eV). Near the antenna region, $n_e$ without and with $B$ are $> 10^{13}$ cm$^{-3}$ for $P > 80$ mTorr and $P > 60$ mTorr, respectively. The space potential $V_{sp}$ ($\sim 11$ V) is nearly constant along the $z$ axis ($z < 45$ cm) and then decreases with $z$ ($V_{sp} \sim 6$ V at $z \sim 75$ cm). When the magnetic field is increased to more than 50 G for the case without FS and with $B$ under low filling pressure, which has been discussed in the previous section, the axial profile behavior as a function of pressure becomes similar to that shown in Fig. 6(b); $I_{is}$ does not decay with $z$ but becomes nearly constant when $P$ is below several tens of mTorr.

In Fig. 6, except for the case with low pressure and with magnetic field (more than few tens of G), $I_{is}$ decays with $z$ and decay length becomes shorter in the higher filling pressure range. This length (15–40 cm) is longer than the mean free path (0.03–3.4 cm), i.e., electron thermal velocity divided by collision frequency, and is also longer than collisional and anomalous skin depth[14] (less than 1 cm) by more than one order of magnitude. Here, electron-electron coulomb collision[16] is also included in addition to the sum of the electron-neutral elastic collision and electron-ion coulomb collision. Nearly constant $I_{is}$ along the $z$ axis may be due to the presence of a propagating wave. Measurements of radial profiles of magnetic fields (three components) at $z = 30$ cm by an interferometric method (Fig. 7) indicate the structure of a helicon excited wave with a dominant azimuthal mode number of $m = 0$. Signals of $B_r$ and $B_\theta$ change signs (polarity) when crossing the plasma center, and the $B_z$ signal becomes maximum at the plasma center, i.e., the observed structure is completely different from those of the $m = 1$ and $-1$ modes. Note that the $B_r$ component is larger compared with a recently obtained value.[17] This comes from the larger (smaller) excited radial region (perpendicular wave number $k_\perp$), which is qualitatively consistent with the theory, i.e., eqs. (48)–(50) in ref. 2, based on a flat density profile. Although plasma is dis-

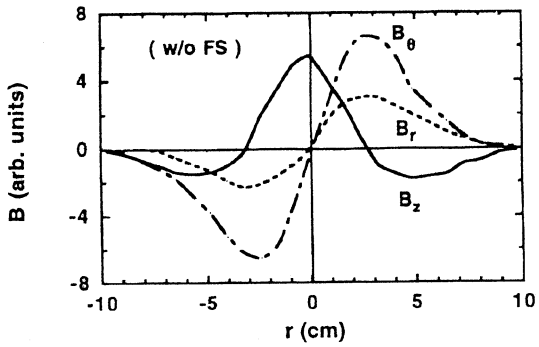


Fig. 7. Radial profiles of excited magnetic fields (radial $B_r$, azimuthal $B_\theta$, and axial $B_z$ components) obtained by interferometric method at $z = 30$ cm with the axial magnetic field $B$ of 72 G and filling pressure $P$ of 27 mTorr, in the absence of the Faraday shield.

tributed throughout the vacuum chamber, the diameter of the excited wave field is limited to $\sim 20$ cm (no excited fields are detected outside this region), which is nearly the same as that of the antenna (18 cm in diameter). Using the present (previous[6]) results, $k_\perp$ is estimated to be $\sim 0.4\,\mathrm{cm}^{-1}$ ($\sim 1.3\,\mathrm{cm}^{-1}$) from radial profiles of the excited fields for a plasma radius of 10 cm (3 cm), and parallel wave number $k_\parallel$ is found to be 0.4–1.2 $\mathrm{cm}^{-1}$ (0.1–0.5 $\mathrm{cm}^{-1}$) using an interferometric method.

Wave measurements, with varying magnetic field and filling pressure both with and without Faraday shields, show good agreement with a theoretical dispersion relation, i.e., plasma angular frequency vs. $k_\parallel$ (if $k_\parallel$ is larger than $k_\perp$, $B/n_e$ is roughly proportional to $k_\parallel^{-2}$). In addition, by changing the phase of the reference wave by the interferometric method, we confirm the existence of a propagating wave (standing wave, i.e., radial structure of the excited wave within $\sim 20$ cm in diameter does not change) character along the axial (radial) direction, which is inherent in a helicon wave. The excitation frequency of 7 MHz lies between the electron and ion cyclotron frequencies in this experiment, which is necessary to excite the helicon wave (this wave is detected above $\sim 20$ G and less than a few-hundreds of G). This is the first excitation of the helicon wave by a spiral antenna, since most of the previous experiments were done using helical, saddle and one-turn antennae wound around the (nonmetal) discharge tube. Needless to say, a lower hybrid wave cannot be a candidate for the propagating wave under this experimental condition, considering the frequency and the propagation direction. Detailed results on the wave phenomena will be published in a separate paper.

Figure 8 shows a comparison of radial $I_{is}$ profiles for cases with and without the magnetic field ($B = 36$ G) in the presence of FS. Removing FS leads to nearly the same results as for the respective cases with and without $B$. When the magnetic field is applied, $I_{is}$ becomes peaked with a large central value due to better radial confinement, as shown in Fig. 8(b). With an increase in $P$, the $I_{is}$ profile becomes peaked for both cases. This can be understood qualitatively by considering radial diffusion and plasma production terms with nearly constant elec-

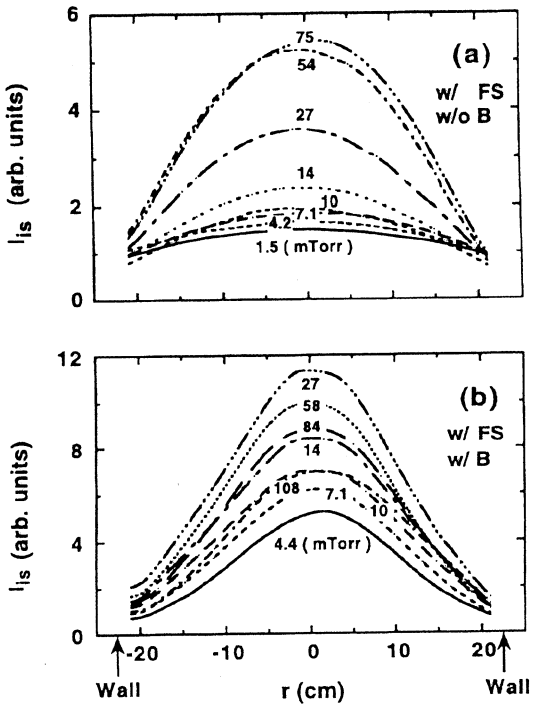


Fig. 8. Radial profiles of ion saturation current $I_{is}$ ($z = 30$ cm, $P_{inp} \sim 2$ kW) for cases (a) without and (b) with the axial magnetic fields $B$ of 36 G, in the presence of the Faraday shield, with various filling pressures $P$.

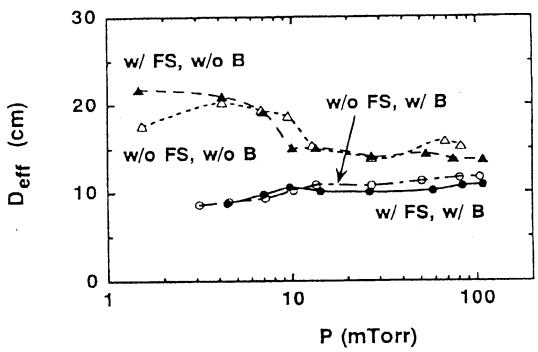


Fig. 9. Effective plasma diameter $D_{eff}$ vs. filling pressure $P$ for the four different cases ($z = 30$ cm, $P_{inp} \sim 2$ kW).

tron temperature (decay length along the axial direction, as shown in Fig. 6, can also be explained by this consideration). When we increase the filling pressure (Fig. 8), the central $I_{is}$ value saturates and then decreases, which is also shown in Fig. 4.

Finally, plasma uniformity, which is an important factor in material processing, is studied, with varying filling pressure $P$, as shown in Fig. 9, based on the data in Fig. 8. Here, effective diameter $D_{eff}$ is defined as the region where $I_{is}$ is uniform within $\pm 5\%$ (if we use the region where $I_{is}$ is uniform within $\pm 3\%$, $D_{eff}$ becomes a few cm smaller). With a low filling pressure $P$ of less than 6 mTorr, $D_{eff}$ is as large as 20–22 cm, whose value normalized by the antenna diameter is $< 1.2$. There is a tendency that $D_{eff}$ decreases with $P$ for cases without $B$ (both with and without FS), whereas $D_{eff}$ with $B$ is smaller due to peaking of the $I_{is}$ profile shown in

Fig. 6, and this $D_{\mathrm{eff}}$ slowly increases with $P$ (both with and without FS). This shows that $B$, which has a small value of less than several tens of G, can be an additional control parameter of the density profile ($I_{\mathrm{is}} \propto n_{\mathrm{e}} T_{\mathrm{e}}^{0.5}$); if the density profile is hollow, applying moderate $B$ can make flatten it.

For the case with FS and $B$, $D_{\mathrm{eff}}$ at $z = 80\,\mathrm{cm}$ is a few cm larger than that measured at $z = 30\,\mathrm{cm}$ ($D_{\mathrm{eff}}$ becomes larger at $P < 2\,\mathrm{mTorr}$ and $P > 60\,\mathrm{mTorr}$). Also at $z = 80\,\mathrm{cm}$, $I_{\mathrm{is}}$, $n_{\mathrm{e}}$ and $T_{\mathrm{e}}$ decrease with filling pressure $P$, in contrast to the trend shown in Fig. 4 ($I_{\mathrm{is}}$ vs. $P$) due to the collision-dominated plasma and relatively long distance from the antenna (source region). $I_{\mathrm{is}}$ also increases with $P_{\mathrm{inp}}$ ($z = 80\,\mathrm{cm}$).

## 5. Conclusions

Effects of the axial magnetic field $B$ and Faraday shield on the performance of RF produced plasma using a four-turn spiral antenna are investigated. The RF power and filling pressure dependences, antenna-plasma coupling, Ar line intensities and spatial profiles of plasma parameters are studied. Except for minor points, no apparent differences between the four cases (with and without the magnetic field and Faraday shield) are found, and impurity lines such as those of silicon, oxygen, iron and nitrogen are not observed at an appreciable level.

Without the Faraday shield and/or with magnetic field, the threshold input power for plasma initiation is lowered and antenna-plasma coupling, i.e., coupling efficiency $\eta$ or plasma loading resistance $R_{\mathrm{p}}$, is improved. This $R_{\mathrm{p}}$ value is consistent with that estimated using collisional and collisionless models, and suggests that there exists a collisionless heating mechanism in the low-pressure (low collisionality) region. With an increase in the applied magnetic field, the ion saturation current $I_{\mathrm{is}}$ increases and its radial profile becomes peaked. In the low-pressure range with $B$, this $I_{\mathrm{is}}$ has a nearly flat profile along the $z$ axis, due mainly to the presence of an excited helicon wave.

1) R. W. Boswell: Plasma Phys. Control. Fusion **26** (1984) 1147.
2) F. F. Chen: Plasma Phys. Control. Fusion **33** (1991) 339.
3) A. Komori, T. Shoji, K. Miyamoto, J. Kawai, and Y. Kawai: Phys. Fluids **B3** (1991) 893.
4) T. Shoji, Y. Sakawa, S. Nakazawa, K. Kadota and T. Sato: Plasma Sources Sci. Technol. **2** (1993) 5.
5) Y. Yasaka and Y. Hara: Jpn. J. Appl. Phys. **33** (1994) 5950.
6) S. Shinohara, Y. Miyauchi and Y. Kawai: Plasma Phys. Control. Fusion **37** (1995) 1015.
7) S. Shinohara and Y. Kawai: Jpn. J. Appl. Phys. **34** (1995) L1571.
8) J. Hopwood: Plasma Sources Sci. Technol. **1** (1992) 109.
9) J. Hopwood, C. R. Guarnieri, S. J. Whitehair and J. J. Cuomo: J. Vac. Sci. Technol. A **2** (1993) 147.
10) J. A. O'Neil, M. S. Barnes and J. H. Keller: Appl. Phys. Lett. **73** (1993) 1621.
11) L. J. Mahoney, A. E. Wendt, E. Barrios, C. J. Richards and J. L. Shohet: J. Appl. Phys. **76** (1994) 2041.
12) J. Amorim, H. S. Maciel and J. P. Sudano: J. Vac. Sci. Techonol. B **9** (1991) 363.
13) Y. Hikosaka, M. Nakamura and H. Sugai: Jpn. J. Appl. Phys. **33** (1994) 2157.
14) M. M. Turner: Phys. Rev. Lett. **71** (1993) 1844.
15) S. C. Brown: *Basic Data of Plasma Physics* (MIT Press, Cambridge, 1966) p. 22.
16) K. Miyamoto: *Plasma Physics for Nuclear Fusion* (MIT Press, Cambridge, Massachusetts, 1988).
17) S. Shinohara, Y. Miyauchi and Y. Kawai: Jpn. J. Appl. Phys. **35** (1996) L731.